Numerical study of the two-dimensional Hubbard model for various band fillings

A. Moreo, D. J. Scalapino, R. L. Sugar, and S. R. White
Department of Physics, University of California–Santa Barbara, Santa Barbara, California 93106

N. E. Bickers
Department of Physics, University of Southern California, Los Angeles, California 90089
and Institute for Theoretical Physics, University of California–Santa Barbara, Santa Barbara, California 93106
(Received 21 August 1989)

Quantum Monte Carlo methods are used to study the physical properties of the two-dimensional Hubbard model for various band fillings. Results for the energy, magnetic moment, magnetic structure factor, and integrated optical spectral weight are presented. A comparison of the half-filled ($\langle n \rangle = 1$) and quarter-filled ($\langle n \rangle = 0.5$) bands is made using results for the momentum distribution $\langle n_k \rangle$, the compressibility K, and the one-electron self-energy $\Sigma(k, i\omega_n)$, which shows that a gap exists in the one-electron excitations at half-filling but is absent for the one-quarter-filled case. At a filling of $\langle n \rangle = 0.87$, the locus of k values for which $\langle n_k \rangle = 0.5$ is found to be close to the free Fermi surface for this filling.

I. INTRODUCTION

In the Hubbard model, the competition between the kinetic and Coulomb energies gives rise to strong electron-electron correlations. In spite of a variety of perturbative and variational calculations, the physical consequences that arise from this competition are not yet fully understood. Here we continue to explore the properties of the two-dimensional (2D) Hubbard model using recently developed quantum Monte Carlo methods.[1] To begin with, in Sec. II, we examine the dependence of kinetic and potential energies on the band filling $\langle n \rangle$ for ratios of the on-site Coulomb energy U to the bandwidth $8t$, ranging from weak to intermediate coupling. The kinetic energy is related to the integral of the optical spectral weight and provides further insight into the behavior of the system as $\langle n \rangle$ is changed. Results for the magnetic structure factor $S(q)$, the electron momentum distribution $\langle n_k \rangle$, and the compressibility K are obtained for lattices with up to 16×16 sites. The behavior of $S(q)$ is discussed for various band fillings, and a detailed comparison of $\langle n_k \rangle$ and K for the half- and quarter-filled cases is made. In addition, the irreducible one-electron self-energy $\Sigma(k, i\omega_n)$ is calculated and shown to provide a useful microscopic probe of the insulating and metallic phases.

It is interesting to contrast the half-filled and quarter-filled bands, and in Sec. III we focus on these two fillings. At half-filling, the electron momentum distribution $\langle n_k \rangle$ appears to be continuous at k_F, while $d\langle n \rangle / d\mu$ vanishes over a range of μ around $\mu = 0$. Both these features are expected for an insulating spin-density wave ground state with a gap in the one-electron spectrum. For the quarter-filled case, the low-temperature variation of $\langle n_k \rangle$ is consistent with the existence of a Fermi surface, and the compressibility appears to be finite. Further microscopic support for this picture is obtained from simulations of the one-electron self-energy $\Sigma(k, i\omega_n)$. The recently developed quantum Monte Carlo techniques provide a natural framework for the numerical calculations of the standard Matsubara thermodynamic Green's functions. These have previously been used to determine various equal-time expectation values as well as static susceptibilities. However, it is also possible to use these same techniques to calculate such quantities as the irreducible one-electron self-energy, and in this way explore the physics contained in selected parts of infinite classes of Feynman graphs.

We conclude Sec. III with results for $\langle n_k \rangle$ for a band filling of $\langle n \rangle = 0.87$. Along with preliminary $\Sigma(k, i\omega_n)$ behavior, the $\langle n_k \rangle$ suggest that at this doping the system is a Fermi liquid, with the locus of points where $\langle n_k \rangle = 0.5$ close to that of the noninteracting system at this same filling. We conclude with a brief summary.

II. ENERGIES AND THE MAGNETIC STRUCTURE FACTOR

We consider the two-dimensional Hubbard model on a square lattice with

$$H = -t \sum_{\langle ij \rangle \sigma} (c^{\dagger}_{i\sigma} c_{j\sigma} + c^{\dagger}_{j\sigma} c_{i\sigma}) + U \sum_i n_{i\uparrow} n_{i\downarrow} \, . \tag{1}$$

In Ref. 1, results for the energy for the half-filled $\langle n \rangle = 1$ case and various U/t values were given. The dependence of the kinetic and potential energies on the band filling $\langle n \rangle$ for various ratios of the interaction to bandwidth, $U/8t$, shows the role of correlations that suppress the double occupancy of a site.

In addition to the energy per site

$$E = \langle H \rangle / N \, , \tag{2}$$

we have calculated the square of the magnetic moment per site

$$\langle (m_i^z)^2 \rangle = \langle (n_{i\uparrow} - n_{i\downarrow})^2 \rangle \ , \tag{3}$$

and the effective one-electron transfer-matrix element

$$\frac{t_{\text{eff}}}{t} = \frac{\langle c_{i\sigma}^\dagger c_{j\sigma} + c_{j\sigma}^\dagger c_{i\sigma} \rangle_U}{\langle c_{i\sigma}^\dagger c_{j\sigma} + c_{j\sigma}^\dagger c_{i\sigma} \rangle_0} \ . \tag{4}$$

The square of the magnetic moment per site is directly related to the probability of double occupancy $\delta = \langle n_{i\uparrow} n_{i\downarrow} \rangle$,

$$\langle (m_i^z)^2 \rangle = \langle n \rangle - 2\delta \ . \tag{5}$$

This probability of double occupancy δ versus $\langle n \rangle$ for various values of U/t is shown in Fig. 1. For $U=0$, $\delta = \langle n \rangle^2/4$, and as U/t increases, δ decreases for all values of $\langle n \rangle$, clearly indicating the role of U in suppressing double occupancy. At the same time, larger values of U/t increase the square of the site magnetization. The enhancement of the mean-square local moment versus $\langle n \rangle$ is shown in Fig. 2. The energy per site E versus $\langle n \rangle$ is plotted in Fig. 3. These results are for a 12×12 lattice with $\beta = 6/t$. Based upon the extrapolations carried out for $\langle n \rangle = 1$ in Ref. 1, we estimate that the systematic error (due to finite $\Delta\tau$, finite β, and finite size) for E in Fig. 3 is less than 5%.

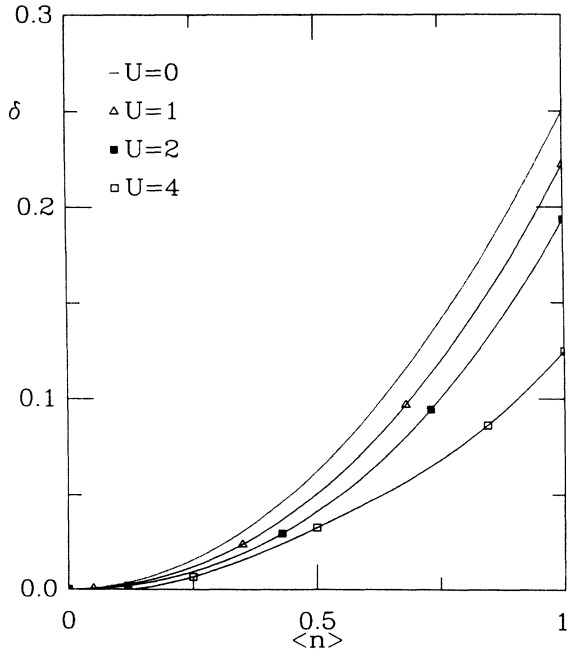

FIG. 1. The probability of double occupancy δ vs the band filling $\langle n \rangle$ for various values of U. In all of the figures we have set $t = 1$.

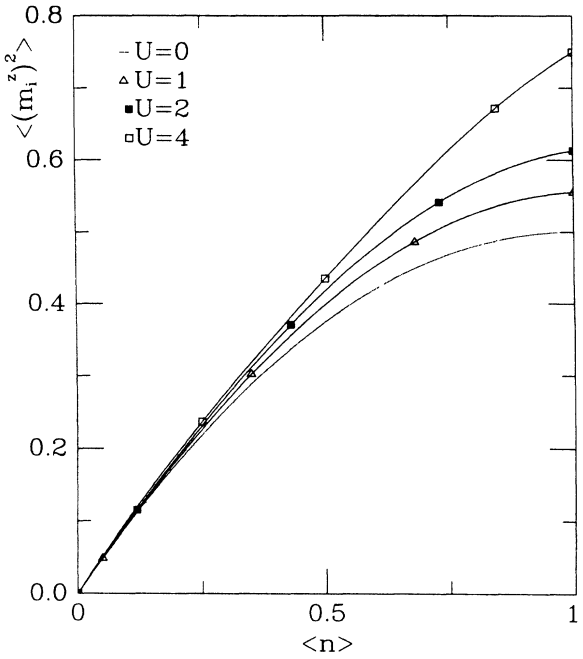

FIG. 2. The mean-square local moment $\langle (m_i^z)^2 \rangle$ vs the band filling $\langle n \rangle$ for various values of U.

For the Hubbard model, Baeriswyl *et al.*[2] have shown that the optical spectral weight $\sigma(\omega)$ is related to the square of the plasma frequency by (f-sum rule)

$$\omega_p^2 = 8 \int_0^\infty d\omega \, \sigma(\omega) = 4\pi e^2 \langle t_x \rangle \ . \tag{6}$$

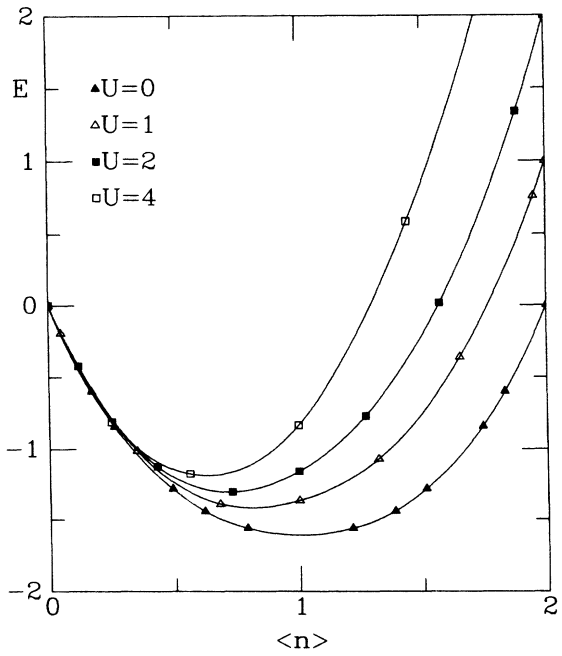

FIG. 3. The energy per site vs $\langle n \rangle$ for different values of U.

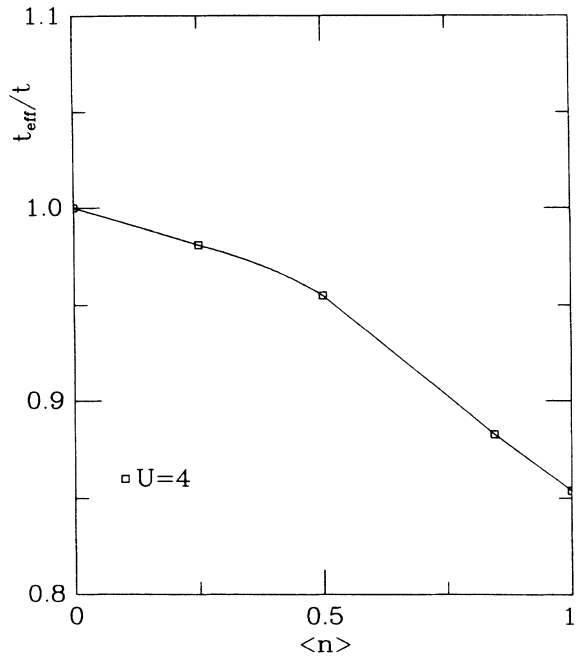

FIG. 4. The effective one-electron transfer matrix element $t_{\rm eff}/t$ vs $\langle n \rangle$ for $U/t=4$.

Here $\langle t_x \rangle = E_0 t_{\rm eff}/4t$, where E_0 is the energy per site for $U=0$ calculated at filling $\langle n \rangle$, and $t_{\rm eff}/t$ is given by Eq. (4). For $\langle n \rangle = 1$, $t_{\rm eff}/t$ decreases as t^2/U for large values of U and ω_p^2 goes to zero.[3] As one dopes away from half-filling, "adding mobile carriers," we expect that the integrated optical spectral weight will increase. As shown in Fig. 4 for $U/t=4$ $t_{\rm eff}/t$ initially increases linearly with $(1-\langle n \rangle)$ as $\langle n \rangle$ changes from 1. Phenomenologically ω_p^2 is given by $4\pi n^* e^2/m^*$ so that one could argue that n^* has an additional hole contribution proportional to $1-\langle n \rangle$; however, it seems more appropriate to say that the effective mass m^* has decreased as vacancies are put into the lattice.

As previously reported,[4,1] a finite-size scaling analysis of the antiferromagnetic structure factor for the half-filled band ($\langle n \rangle = 1$) implies that the ground state has long-range antiferromagnetic order. At weak to moderate values of U/t ($U/t < 8$), this state may best be described as a spin-density wave state, while when U exceeds the bandwidth, a description in terms of an antiferromagnetic Heisenberg model with $J=4t^2/U$ is more appropriate. In both cases, the magnetic structure factor $S(\mathbf{q})$, defined as

$$S(\mathbf{q}) = \frac{1}{N} \sum_l e^{i\mathbf{q}\cdot\mathbf{x}_l} \langle m_{i+l}^z m_i^z \rangle \ , \tag{7}$$

peaks at $\mathbf{q}=(\pi,\pi)$ diverging as the system size N and the inverse temperature β go to infinity. At low temperatures, when the system is initially doped away from half-filling, a random-phase approximation[5] (RPA) predicts the formation of an incommensurate spin-density wave state with wave vector $\mathbf{Q}_x=(\pi-\Delta q,\pi)$ or $\mathbf{Q}_y=(\pi,\pi-\Delta q)$, with $\Delta q=\mu/t$ at $T=0$. When the doping exceeds a critical value (e.g., $\langle n \rangle = 0.85$ for $U/t=2$), the system becomes paramagnetic. A conserving approximation[6] predicts the following features as a function of temperature and doping in the intermediate coupling range ($U/t \simeq 4$): (a) for fillings between 1 and approximately 0.94, a finite-temperature crossover from a high-temperature paramagnetic phase to a low-temperature commensurate phase (with "nearly" long-range order); and (b) for fillings between 0.94 and approximately 0.82, a crossover from a paramagnetic phase to a d-wave superconducting phase. (This work did not investigate the crossover between the commensurate phase and possible incommensurate phases which presumably occurs near half-filling for $T \to 0$.) Both the RPA and the conserving approximation imply that when the peak in the magnetic structure factor moves from (π,π), it moves along $(\pi-\Delta q,\pi)$ or $(\pi,\pi-\Delta q)$ rather than simply moving in along the diagonal $(\pi-\Delta q,\pi-\Delta q)$.

To explore this, we have studied the behavior of $S(\mathbf{q})$ as a function of doping.[7] In Figs. 5(a)–5(c) we show results for $S(\mathbf{q})$ obtained on an 8×8 lattice with $U/t=4$, $\beta=6/t$, and $\langle n \rangle = 1$, 0.83, and 0.72. The solid line was obtained from a simple interpolation. At half-filling, $S(\mathbf{q})$ clearly peaks at (π,π). Decreasing the filling to $\langle n \rangle = 0.83$, we observe a much smaller peak that appears to have shifted out along the $(\pi,\pi-\Delta q)$ edge, with $\Delta q \cong 0.3$, rather than down along the diagonal $(\pi-\Delta q,\pi-\Delta q)$. The results are symmetric with the same form observed along the $(\pi-\Delta q,\pi)$ axis not shown in the figures. Thus, the simulation results are consistent with the peak at (π,π) splitting into two peaks, as predicted by the RPA analysis[5] and conserving approximation studies.[6] For $\langle n \rangle = 0.72$ we find a still smaller peak, as shown in Fig. 5(c), with a larger value of Δq [using the interpolation shown in Fig. 5(c) one finds $\Delta q \approx 0.4$]. Decreasing $\langle n \rangle$ further, it appears that the maxima in $S(q)$ moves towards $(\pi,0)$ and $(0,\pi)$, although they become very weak.[8] We observed related behavior on 4×4 and 6×6 lattices, but on these smaller lattices it is naturally even more difficult to determine details of the Δq shifts. It is clear, however, that $S(\mathbf{q})$ peaks along $(\pi,\pi-\Delta q)$ and $(\pi-\Delta q,\pi)$ rather than the diagonal $(\pi-\Delta q,\pi-\Delta q)$ or at (π,π).

A key question, of course, is to determine whether these peaks in $S(\mathbf{q})$ diverge for $\langle n \rangle < 1$ as the lattice size and inverse temperature are increased. Over the temperature range presently accessible to us, $\beta \lesssim 6/t$, we find no evidence indicating the growth of long-range incommensurate order. Unfortunately, we are presently unable to go to lower temperatures for the densities of interest (e.g., $\langle n \rangle = 0.7$–0.9) because of calculational problems associated with fluctuations in the signs of the fermion determinants. As previously discussed,[1] this sign problem is absent for $\langle n \rangle = 1$ and causes minimal difficulties for $\langle n \rangle \leq 0.6$. Thus, in the following we turn to a comparison of the half-filled ($\langle n \rangle = 1$) and quarter-filled ($\langle n \rangle = 0.5$) cases. Having studied these two limits, we will return to an intermediate filling, $\langle n \rangle = 0.87$, at the end of the next section.

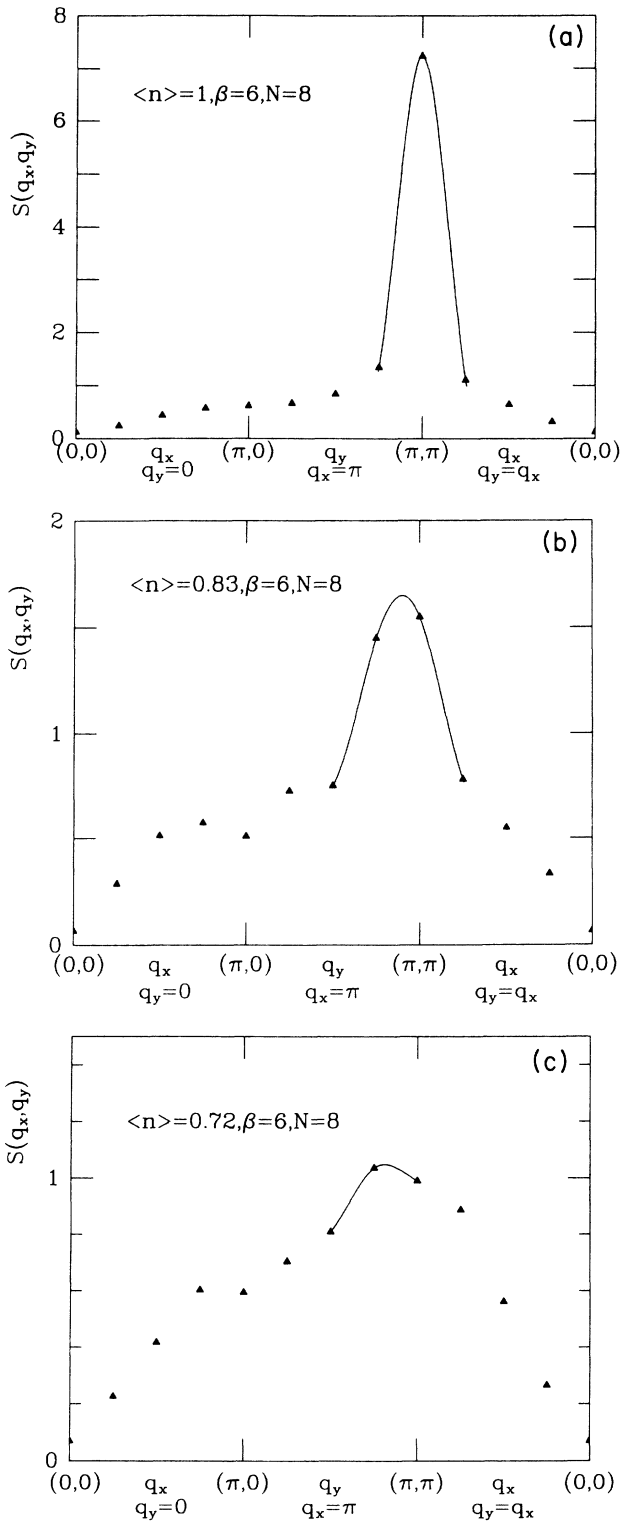

FIG. 5. $S(q_x,q_y)$ vs (q_x,q_y) on an 8×8 lattice with $U/t=4$, $\beta=6/t$, and (a) $\langle n\rangle=1$, (b) $\langle n\rangle=0.83$, and (c) $\langle n\rangle=0.72$. The solid line is a fit to guide the eye.

III. MOMENTUM DISTRIBUTION COMPRESSIBILITY, AND $\Sigma(k_F,i\omega_n)$

In order to obtain further insight into the nature of the correlations in the antiferromagnetic $\langle n\rangle=1$ and paramagnetic $\langle n\rangle=0.5$ states, we have calculated the momentum distribution $\langle n_k\rangle$, the compressibility K, and the one-electron self-energy. All of these can be obtained from the one-electron Green's function,

$$G_{ij}(\tau)=-\langle Tc_i(\tau)c_j^\dagger(0)\rangle \tag{8}$$

which, along with the energy, has the smallest statistical fluctuations of the quantities evaluated in our Monte Carlo simulations. Thus we are able to obtain reliable information for these one-electron properties on larger lattices. This is very important for the momentum distribution $\langle n_k\rangle$, where the spacing of the allowed momenta depends on the lattice size.

The electron momentum distributions $\langle n_k\rangle$ for a half-filled and quarter-filled band with $U/t=4$ and $\beta=6/t$ are shown in Figs. 6 and 7. Here $k=k_x=k_y$, so that Figs. 6 and 7 show $\langle n_k\rangle$ with $\mathbf{k}$ along the (1,1) direction. The solid line shown in Figs. 6(a) and 7(a) is the noninteracting Fermi function

$$f(\epsilon_k)=\{\exp[-\beta(\epsilon_k-\mu)]+1\}^{-1}$$

with

$$\epsilon_k=-2t(\cos k_x+\cos k_y)$$

and μ is adjusted to give $\langle n\rangle=1$ and 0.5, respectively. The open triangles are for a 16×16 lattice. The remaining triangles are from different sized lattices ranging from 6×6 to 14×14.

At $T=0$, a mean-field spin-density wave approximation gives

$$\langle n_k\rangle_{mf}=\tfrac{1}{2}\left[1-\frac{\epsilon_k}{E_k}\right] \tag{9}$$

with $E_k=(\epsilon_k^2+\Delta^2)^{1/2}$, where Δ is determined by

$$\frac{1}{U}=\frac{1}{N}\sum_k\frac{1}{E_k}\ . \tag{10}$$

For $U/t=4$, Eq. (10) gives $\Delta/t=1.38$. The mean-field prediction $\langle n_k\rangle_{mf}$, Eq. (9), is compared with the Monte Carlo results for $\langle n_k\rangle_{\rm MC}$ in Fig. 6(b). While the mean-field result gives a reasonable qualitative fit to $\langle n_k\rangle$, it is clear that the mean-field gap is too large, causing $\langle n_k\rangle_{mf}$ to lie below $\langle n_k\rangle_{\rm MC}$ for k values near $\pi/2$. Fluctuations are known to reduce Δ.[9] The dashed curve in Fig. 6(b) shows Eq. (9) for $\langle n_k\rangle$ with $\Delta=1.15$, which gives a better fit near $\pi/2$.

For the quarter-filled case, we have evaluated the lowest-order self-energy graph shown in Fig. 8:

$$\Sigma(k,i\omega_n)=\frac{U^2}{N^2}\sum_{p,q}\frac{f(\epsilon_p)-f(\epsilon_{k-q})f(\epsilon_p)-f(\epsilon_{p+q})f(\epsilon_p)+f(\epsilon_{k-q})f(\epsilon_{p+q})}{i\omega_n-(\epsilon_{k-q}+\epsilon_{p+q}-\epsilon_p)}\ . \tag{11}$$

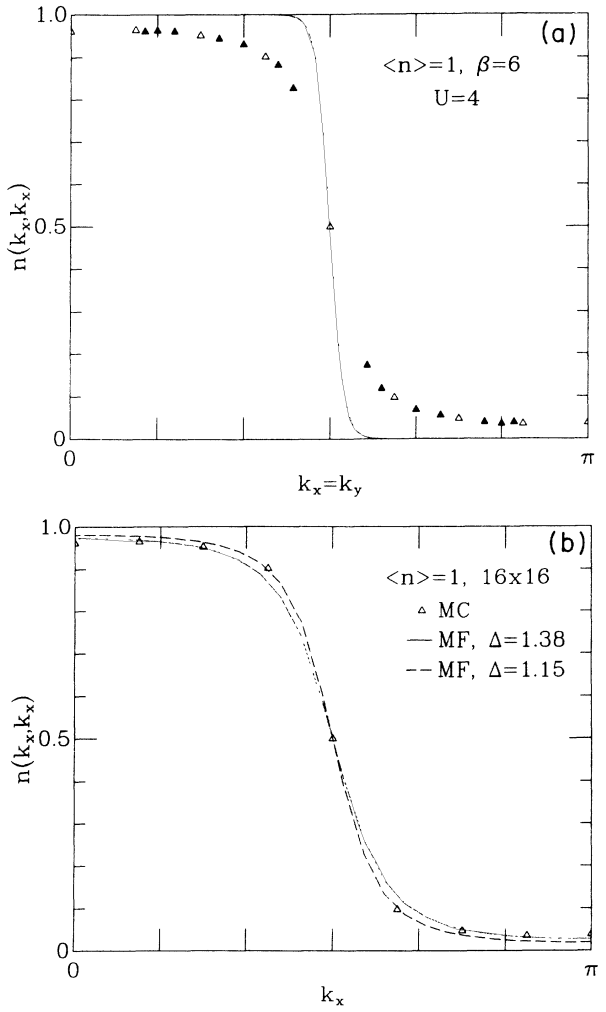

FIG. 6. The momentum distribution $\langle n_k \rangle$ vs $\mathbf{k}=(k_x,k_x)$ for $\langle n \rangle=1$. Here $U/t=4$ and $\beta=6/t$. (a) Results for $6\times6,\ldots,16\times16$ lattices are shown. The open triangles are for the 16×16 lattice. The solid line is the Fermi function for a half-filled, noninteracting system at a temperature $\beta=6/t$. (b) Monte Carlo results for a 16×16 lattice, shown as open triangles, are compared with the predictions of mean-field spin-density wave approximation.

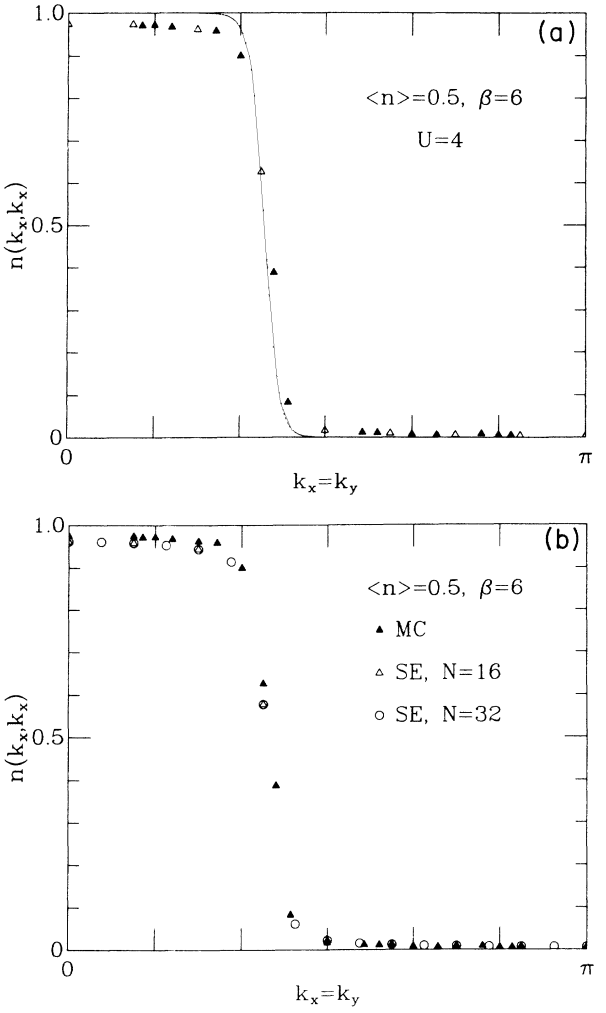

FIG. 7. The momentum distribution $\langle n_k \rangle$ vs $\mathbf{k}=(k_x,k_x)$ for $\langle n \rangle=0.5$. As in Fig. 6, $U/t=4$ and $\beta=6/t$. (a) Results for $6\times6,\ldots,16\times16$ lattices are shown with the open triangles corresponding to the 16×16 lattice. The solid line is the Fermi function for a quarter-filled band at $\beta=6/t$. (b) Comparison of the Monte Carlo results solid triangles with the results for $\langle n_k \rangle$ obtained by keeping the lowest-order self-energy graph shown in Fig. 8.

Here $f(\epsilon_k)$ is the usual Fermi function, and $\omega_n=(2n+1)\pi T$ is a fermion Matsubara frequency. The momentum distribution can be expressed as

$$\langle n_k \rangle = T \sum_n e^{-i\omega_n 0^-} G_k(i\omega_n) , \tag{12}$$

where 0^- represents an infinitesimal number less than 0. Adding and subtracting the noninteracting result provides a convenient form for the numerical evaluation of $\langle n_k \rangle$; we have

$$\langle n_k \rangle = f(\epsilon_k) + T \sum_n \frac{\Sigma(i\omega_n,k)}{(i\omega_n-\epsilon_k)[i\omega_n-\epsilon_k-\Sigma(k,i\omega_n)]} . \tag{13}$$

Using the lowest-order self-energy, Eq. (11), we have calculated $\langle n_k \rangle$ from Eq. (13) for a 16×16 and 32×32 lattice with $\langle n \rangle=0.5$, $U/t=4$, and $\beta=6/t$. The results are in reasonable agreement with the Monte Carlo data as shown in Fig. 7(b).

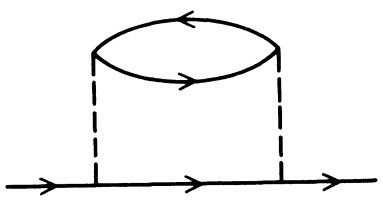

FIG. 8. The lowest-order self-energy graph for a Hubbard model.

Another probe of the electronic correlations and the metallic or insulating character of the system is the compressibility

$$K=\frac{1}{\langle n\rangle^2}\frac{d\langle n\rangle}{d\mu} . \tag{14}$$

Here $\langle n\rangle$ is the average site occupation for a given chemical potential. For a noninteracting ($U=0$) 2D Hubbard model on a square lattice

$$K=\frac{2}{NT}\sum_k f(\epsilon_k)[1-f(\epsilon_k)] . \tag{15}$$

At low temperatures $K=N(\mu)$, where $N(\mu)$ is the density of states at μ. Near half-filling $\mu\to 0$, the saddle points at the corners of the Fermi surface give rise to a logarithmic Van Hove singularity, and

$$N(\mu)\simeq\frac{\ln(16t/\mu)}{\pi^2 t} . \tag{16}$$

Because of this, K diverges for the noninteracting system as $\mu\to 0$. However, the interacting $U\neq 0$ system has been

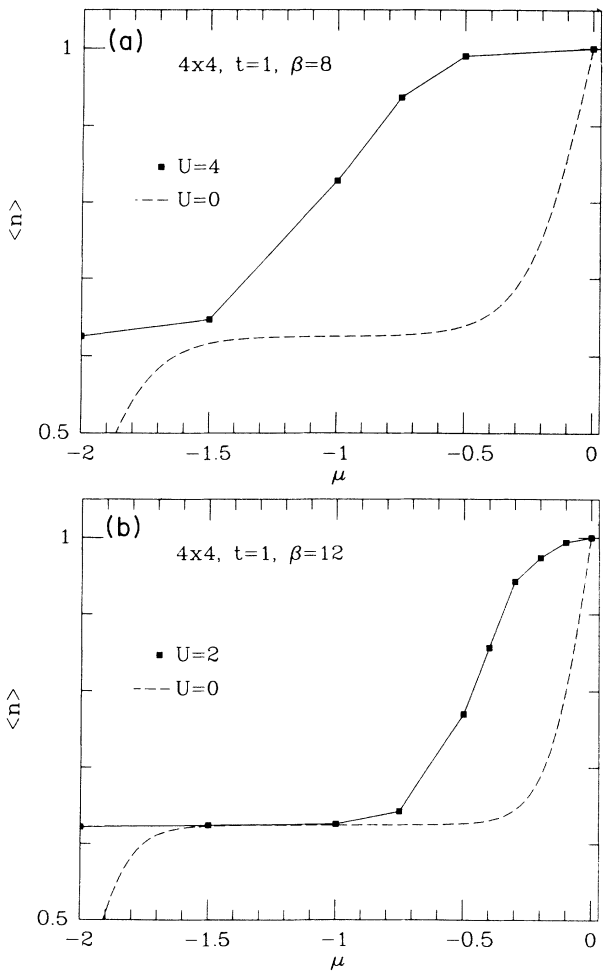

FIG. 9. The average electron occupation per site $\langle n\rangle$ vs μ on a 4×4 lattice. The dashed line is for $U=0$ and the points are Monte Carlo results for (a) $U/t=4$ and $\beta=8/t$, and (b) $U/t=2$ and $\beta=12/t$.

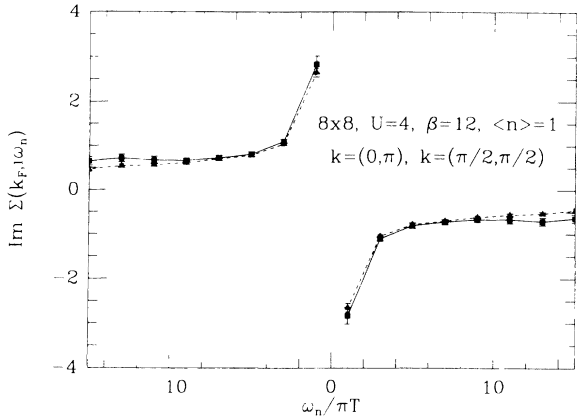

FIG. 10. The imaginary part of the self-energy $\Sigma(k_F,i\omega_n)$ vs $\omega_n/\pi T$ for a half-filled band ($\langle n\rangle=1$) and $k_F=(0,\pi)$ (squares) and $k_F=(\pi/2,\pi/2)$ (triangles). These results were obtained from Monte Carlo runs on an 8×8 lattice with $U/t=4$ and $\beta=12/t$.

shown to exhibit long-range antiferromagnetic order, and as we have seen, the behavior of $\langle n_k\rangle$ is consistent with the occurrence of a gap. In this case, we expect $d\langle n\rangle/d\mu$ to vanish. In Figs. 9(a) and 9(b) we show $\langle n\rangle$ versus μ for $U/t=4$ and 2. The dashed line shows the $U=0$ result. Similar results are also found for $U/t=1$. It therefore appears that when $U\neq 0$, $dn/d\mu$ vanishes as $\mu\to 0$.

As discussed, the quantum Monte Carlo method generates the standard thermodynamic, temperature-ordered Green's functions. Thus, for example, we can calculate the one-electron Green's function

$$G(k,\tau)=-\langle Tc_k(\tau)c_k^\dagger(0)\rangle \tag{17}$$

with $c_k(\tau)=e^{H\tau}c_k e^{-H\tau}$ by simply taking the spatial Fourier transform of Eq. (8). Then, taking the τ-Fourier transform of $G(k,\tau)$ at the fermion Matsubara frequencies $\omega_n=(2n+1)\pi T$, we have

$$G(k,i\omega_n)=\int_0^\beta e^{i\omega_n\tau}G(k,\tau)d\tau . \tag{18}$$

The irreducible electron self-energy $\Sigma(k,i\omega_n)$ can then be determined from the Dyson equation

$$\Sigma^{-1}(k,i\omega_n)=G^{-1}(k,i\omega_n)-i\omega_n-(\epsilon_k-\mu) . \tag{19}$$

We have carried out Monte Carlo calculations of $G_{ij}(\tau)$ and then determined $\Sigma(k,i\omega_n)$. At half-filling, $\epsilon_k=0$ and in this case, $\Sigma(k_F,i\omega_n)$ is pure imaginary. Figure 10 shows $\mathrm{Im}\Sigma(k_F,i\omega_n)$ with $k_F=(0,\pi)$ and $(\pi/2,\pi/2)$, plotted versus $\omega_n/\pi T$, for an 8×8 lattice with $\beta=12/t$ and $U/t=4$. This can be compared with $\mathrm{Im}[\Sigma(k_F,i\omega_n)]$, with $k_F=(\pi/4,\pi/2)$, and for a quarter-filled band with $\beta=8/t$ and $U/t=4$, shown in Fig. 11.

For a normal Fermi liquid it is useful to write the imaginary part of Σ in the form

$$\Sigma(k,i\omega_n)=[1-Z(k,i\omega_n)]i\omega_n . \tag{20}$$

At low temperatures with $k=k_F$, $Z(k_F,i\pi T)>1$ is the

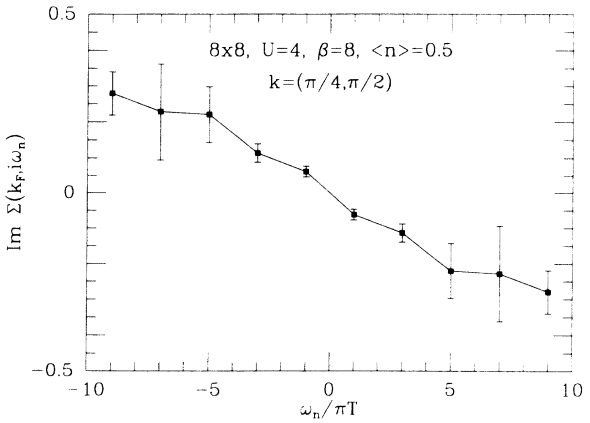

FIG. 11. The imaginary part of the self-energy $\Sigma(k_F,i\omega_n)$ vs $\omega_n/\pi T$ for a quarter-filled band ($\langle n\rangle=0.5$) with $k_F=(\pi/4,\pi/2)$. These results were obtained from Monte Carlo runs on an 8×8 lattice with $U/t=4$ and $\beta=8/t$.

quasiparticle wave function renormalization parameter. Thus, as seen in Fig. 11, we expect that for a Fermi liquid, the imaginary part of $\Sigma(k_F,i\omega_n)$ will have a negative slope for small values of ω_n. In perturbation theory, the leading contribution to Σ, Eq. (11), is plotted in Fig. 12. The perturbation theory result is in good agreement with the Monte Carlo data for $\langle n\rangle=0.5$ and clearly indicates a Fermi-liquid-like behavior.

Alternatively, for the half-filled case in which Monte Carlo simulations show that long-range antiferromagnetic correlations develop in the ground state, we expect that there will be a gap in the one-electron spectrum. In mean-field theory[9]

$$\Sigma(k,i\omega_n)=\frac{\Delta^2}{i\omega_n+\epsilon_k}\ , \tag{21}$$

with Δ given by Eq. (10). Then when k is put on the Fermi surface and $\epsilon_k=0$, we expect $\mathrm{Im}\Sigma(k_F,i\omega_n)$ $\sim-\Delta^2/\omega_n$. This is what is qualitatively seen in the Monte Carlo data shown in Fig. 10. We conclude that the behavior of $\Sigma(k,i\omega_n)$, which can be directly obtained from the Monte Carlo calculation, can provide information on the formation of a gap.

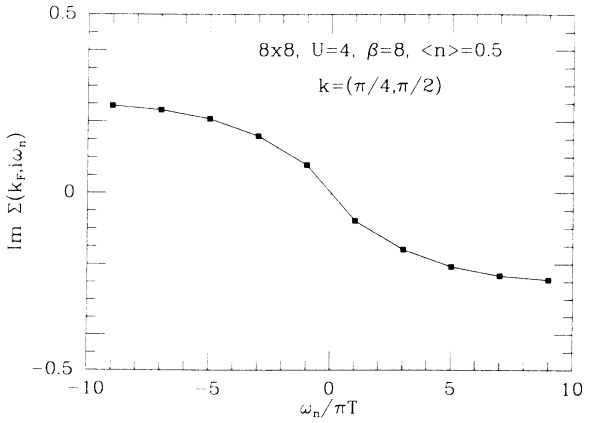

FIG. 12. The imaginary part of the lowest-order self-energy graph (Fig. 8) vs ω_n for $k_F=(\pi/4,\pi/2)$ for $\langle n\rangle=0.5$. These results were calculated from Eq. (11) for an 8×8 lattice with $U/t=4$ and $\beta=8/t$ in order to compare with the Monte Carlo results shown in Fig. 11.

Thus the Monte Carlo data on $\langle n_k\rangle$ and $\Sigma(k,i\omega_n)$ support the notion that the half-filled band has a gap at the noninteracting Fermi surface, while the quarter-filled band is a normal fermi liquid (at least within the temperature and momentum resolution of our simulations). With this in mind, we returned to the important problem of what happens when the system is only doped slightly off half-filling, e.g., $\langle n\rangle=0.87$. As previously noted, the fermion determinantal sign problem makes it difficult to go to low temperatures at such fillings. However, we were able to obtain some data with $\langle n\rangle=0.87$ on a 16×16 lattice with $U/t=4$ and $\beta=6/t$. Results for $\langle n_k\rangle$ are shown in Fig. 13. Here the Brillouin zone of allowed k values is shown and a solid square is put at k points where $\langle n_k\rangle>0.5$. Then extrapolating from the measured $\langle n_k\rangle$ to determine values of k in the Brillouin zone where $\langle n_k\rangle=0.5$ gives the $\times$'s shown in Fig. 13. For comparison, the solid line is the noninteracting $U=0$ Fermi surface for $\langle n\rangle=0.87$, while the dashed line is the $U=0$ Fermi surface for $\langle n\rangle=1.0$. Finally, limited data on $\Sigma(k,i\omega_n)$ for $\langle n\rangle=0.87$ gave no indication of the formation of a spin-density wave gap for k points where $\langle n_k\rangle$ was near 0.5.

IV. CONCLUSION

Using quantum Monte Carlo techniques, we have continued our study of the two-dimensional Hubbard model.

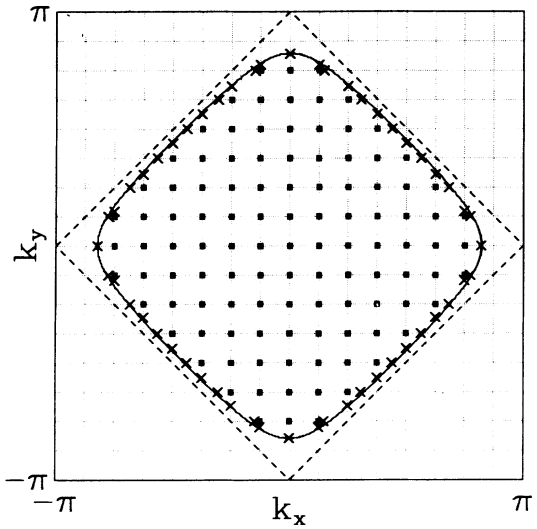

FIG. 13. This shows the allowed k points in the Brillouin zone for a 16×16 lattice. The solid squares mark k points at which $\langle n_k\rangle>0.5$ for a band filling of $\langle n\rangle=0.87$ with $U/t=4$ and $\beta=6/t$. Extrapolating the Monte Carlo data for $\langle n_k\rangle$ on the 16-site lattice to the points in the Brillouin zone where $\langle n_k\rangle$ would equal 0.5 gives the crosses ($\times$). The solid line is the noninteracting ($U=0$) Fermi surface for $\langle n\rangle=0.87$ and the dashed line is the noninteracting Fermi surface for the half-filled band $\langle n\rangle=1.0$.

At half-filling and low temperatures we find evidence in $\langle n_k \rangle$, K, and $\Sigma(k_F, i\omega_n)$ for a one-electron gap. This is consistent with the existence of long-range antiferromagnetic order in the ground state. As the system is doped away from half-filling, the peak in the magnetic structure factor is found to split, moving along $(\pi - \Delta q, \pi)$ and $(\pi, \pi - \Delta q)$. It also becomes much weaker, and over the temperature regime and for the lattice size that we can simulate, we do not find evidence for long-range incommensurate magnetic order.

For $\langle n \rangle = 0.5$, corresponding to a quarter-filled band, the system appears to be in a Fermi-liquid state. The one-electron momentum distribution sharpens relative to the $\langle n \rangle = 1$ case, and the self-energy varies linearly with ω_n, having a negative slope as $\omega_n \to 0$. For $\langle n \rangle = 1.0$, the one-electron momentum distribution does not sharpen and is consistent with the mean-field spin-density-wave (SDW) result using a reduced value of the gap. In addition, the compressibility changes from being infinite to going to zero in the presence of U. A clear signature of a gap is also seen in $\Sigma(k, i\omega_n)$, which diverges as $1/\omega_n$ as $\omega_n \to 0$.

While determinantal sign problems make it difficult to go to low temperatures at fillings near half-filling, calculations of $\langle n_k \rangle$ for $\langle n \rangle = 0.87$ show that the locus of k values where $\langle n_k \rangle = 0.5$ is close to the noninteracting Fermi surface for this filling. Furthermore, limited data on $\Sigma(k, i\omega_n)$ showed no evidence for a spin-density wave gap near the $\langle n_k \rangle = 0.5$ locus of k points. However, as noted in Sec. II, the integrated optical spectral weight shows the effect of U in altering the effective (n/m) value that enters the f-sum rule. In addition, we have previously found that there is an attractive pairing vertex in the two-particle d wave channel at this filling. What happens at temperatures lower then 1/50 of the bandwidth for $\langle n \rangle = 0.87$ remains unresolved.

ACKNOWLEDGMENTS

We wish to thank V. Emery, S. Kivelson, E. Loh, A. Millis, and J. R. Schrieffer for their insight and interest. This work was supported in part by National Science Foundation Grants No. DMR86-15454 and No. PHY86-14185. S.R.W. gratefully acknowledges the support of IBM. The numerical calculations reported in this paper were performed on the Cray XMP at the San Diego Supercomputer Center (SDSC). We wish to thank SDSC for its support.

[1] S. R. White, D. J. Scalapino, R. L. Sugar, E. Y. Loh, J. E. Gubernatis, and R. T. Scalettar, Phys. Rev. B **40**, 506 (1989). This paper gives a description of the Monte Carlo procedure and a detailed discussion of the half-filled band.

[2] D. Baeriswyl, C. Gros, and T. M. Rice, Phys. Rev. B **35**, 8391 (1986). We want to particularly thank A. Millis for bringing this reference to our attention and for discussions regarding the optical spectral weight.

[3] See Fig. 7, and the accompanying discussion in Ref. 1.

[4] J. E. Hirsch and S. Tang, Phys. Rev. Lett. **62**, 591 (1989).

[5] H. J. Schulz (unpublished).

[6] N. E. Bickers, D. J. Scalapino, and S. R. White, Phys. Rev. Lett. **62**, 961 (1989).

[7] Incommensurate structure in Monte Carlo simulations of $S(q)$ has been reported by M. Imada and Y. Hatsugai, J. Phys. Soc. Jpn. (to be published).

[8] A similar behavior has been observed in spin systems with frustration; see E. Dagotto and A. Moreo, Phys. Rev. B **39**, 4744 (1989); Phys. Rev. Lett. **63**, 2148 (1989).

[9] J. R. Schrieffer, X.-G. Wen, and S. Zhang, Phys. Rev. B **39**, 11 663 (1989).